Wind Energy

WIND ENERGY
Wind Energ. 2015; **18**:111–132
Published online 15 November 2013 in Wiley Online Library (wileyonlinelibrary.com). DOI: 10.1002/we.1686

RESEARCH ARTICLE

Two improvements to the dynamic wake meandering model: including the effects of atmospheric shear on wake turbulence and incorporating turbulence build-up in a row of wind turbines

Rolf-Erik Keck[1,2], Martin de Maré[1,2], Matthew J. Churchfield[3], Sang Lee[3], Gunner Larsen[2] and Helge Aagaard Madsen[2]

[1] Rotor Systems, Vestas Wind Systems A/S, 4000 Roskilde, Denmark
[2] Wind Energy Department, Risø DTU National Laboratory for Sustainable Energy, 4000 Roskilde, Denmark
[3] National Renewable Energy Laboratory, 15031 Denver West Parkway, Golden, Colorado 80401-3305, USA

ABSTRACT

The dynamic wake meandering (DWM) model is an engineering wake model designed to physically model the wake deficit evolution and the unsteady meandering that occurs in wind turbine wakes. The present study aims at improving two features of the model:

1. The effect of the atmospheric boundary layer shear on the wake deficit evolution by including a strain-rate contribution in the wake turbulence calculation.
2. The method to account for the increased turbulence at a wake-affected turbine by basing the wake-added turbulence directly on the Reynolds stresses of the oncoming wake. This also allows the model to simulate the build-up of turbulence over a row of turbines in a physically consistent manner.

The performance of the modified model is validated against actuator line (AL) model results and field data from the Lillgrund offshore wind farm. Qualitatively, the modified DWM model is in fair agreement with the reference data. A quantitative comparison between the mean flow field of the DWM model with and without the suggested improvements, to that of the AL model, shows that the root-mean-square difference in terms of wind speed and turbulence intensity is reduced on the order of 30% and 40%, respectively, by including the proposed corrections for a row of eight turbines. Furthermore, it is found that the root-mean-square difference between the AL model and the modified DWM model in terms of wind speed and turbulence intensity does not increase over a row of turbines compared with the root-mean-square difference of a single turbine. Copyright © 2013 John Wiley & Sons, Ltd.

KEYWORDS

Dynamic wake meandering; DWM; Wake modelling; Actuator line model; Wind turbine wake; wake-added turbuelnce; Wake turbulence; Wind farm modelling

Correspondence

Rolf-Erik Keck, Wind Energy Department, Risø DTU National Laboratory for Sustainable Energy, DK 4000 Roskilde.
E-mail: rolf.keck@gmail.com

Received 27 July 2012; Revised 2 July 2013; Accepted 3 October 2013

1. INTRODUCTION

The dynamic wake meandering (DWM) model (Madsen *et al.*[1]) is a reduced-order wake model developed to capture the most important physical effects of wind turbine wake dynamics while maintaining low computational demand, making it suitable for design calculations. The current form of the DWM model consists of three separate parts, which are outlined in the succeeding text and shown in Figure 1:

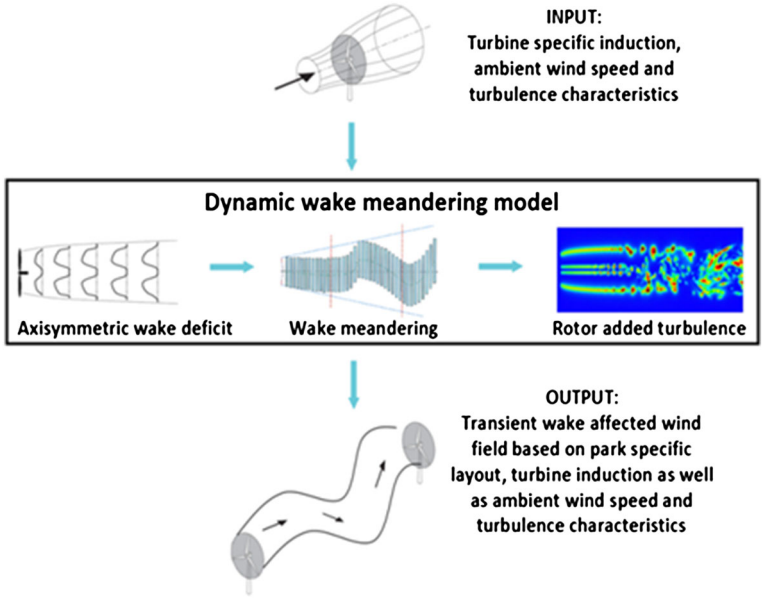

Figure 1. An overview of the workflow of the DWM model.

1. A steady-state, axisymmetric wake deficit is calculated on the basis of the thin shear layer approximation to the Navier–Stokes (N–S) equations, as proposed by Ainslie.[2,3]
2. Stochastic, large-scale meandering of the wake deficit is applied. The wake deficit is assumed to act as a passive tracer that is translated horizontally and vertically by large-scale atmospheric turbulent fluctuations (eddies larger than twice the turbine rotor diameter), as suggested by Larsen *et al.*[4]
3. Small-scale wake-added turbulence is superimposed on the flow field that results from parts 1 and 2. The magnitude of the wake-added turbulence is based on the local depth and the radial gradient of the wake deficit (for further details, see Madsen *et al.*[5]). In the current formulation, the wake-added turbulence only affects the loads at the downstream rotors. No coupling to the velocity and turbulence evolution of the wake of the downstream turbine is included.

The resulting wake dynamics are applied as input to an aeroelastic calculation to simulate the effects of operating a turbine in the wakes of others, as described by Madsen *et al.*[6] In practice, the shape of the wake deficit is determined by the ambient wind speed and turbulence intensity, along with the turbine induction and distance between the wake-receiving and wake-emitting turbines. The small-scale turbulence is based on the distance from the wake centre and is superimposed onto the wake deficit in the meandering frame of reference (MFoR). Both of these contributions to the wake effects are time invariant. The dynamic effect in the DWM model is then created by the large-scale translation of the entire deficit, including the small-scale turbulence. The meandering is applied in the vertical and lateral directions only. Finally, the atmospheric shear is taken into account by superimposing the vertical shear profile on the calculated wake dynamics. The downstream rotor will therefore experience a sheared inflow, on which the mean wake deficit and the added small-scale turbulence are superimposed. The location of the wake deficit relative to the rotor is updated at every time step of the aeroelastic simulation.

In the current DWM formulation, the effect of atmospheric shear is added to the mean flow field only once the wake deficit has been calculated. A focus of this paper is to include the effect of atmospheric shear-generated turbulence in the wake deficit calculation of the DWM model. This results in a more accurate wake deficit development in the far-wake region, where the vertical atmospheric wind shear is of the same order of magnitude or larger than the wake deficit shear and therefore is a non-negligible source of turbulence kinetic energy generation in the wake. The more comprehensive modelling of the far-wake turbulence dynamics also enables a more physically consistent wake-added turbulence formulation based on the turbulent stresses in the wake deficit calculations. Using the improved wake-added turbulence description, we also propose a method to include the wake-added turbulence from upstream wakes in the calculation of the wake deficit of a downstream rotor. This enables the DWM to simulate the mean flow field and the build-up of turbulence over a row of turbines in a more physically consistent manner.

The first section of the paper describes the method used to calculate the wake deficit in the DWM model. This is followed by a brief summary of the computational fluid dynamics (CFD) actuator line (AL) models used for validating the proposed DWM model improvements. The two following sections give the physical motivation and theory for

DOI: 10.1002/we

including a contribution from atmospheric shear on the wake turbulence, along with a suggestion on how to practically include the effect in DWM calculations over a row of turbines. Finally, we present the results, discussion and conclusion of the work.

1.1. The deficit calculations in the DWM model

The wake deficit in the DWM model is governed by the steady-state, axisymmetric thin shear layer approximation of the N–S equations in which momentum is given by

$$u\frac{\partial u}{\partial x}+v\frac{\partial u}{\partial r}=\frac{1}{r}\frac{\partial}{\partial r}\left(\upsilon_T r\frac{\partial u}{\partial r}\right) \tag{1}$$

and continuity is maintained through

$$\frac{1}{r}\frac{\partial}{\partial r}(rv)+\frac{\partial u}{\partial x}=0. \tag{2}$$

In these equations, the velocity components u and v are in the mean flow (x) and radial (r) directions, respectively, and v_t is an eddy viscosity. The main benefit in using the thin shear layer approximation is a significantly reduced computational cost. This is achieved by omitting the pressure gradient term, approximating the flow as axisymmetric and assuming that the magnitude of the velocity gradients in streamwise direction is much smaller than those in radial direction. The fact that the pressure gradient is neglected means that there is no pressure–velocity coupling and no need to solve an equation for pressure, which is often the most expensive part of the solution procedure. Further, as the flow is assumed to be axisymmetric, only one component of the momentum equation needs to be solved and the other velocity component is given by the continuity equation (which is otherwise unused, as there is no pressure–velocity coupling). Turbulent diffusion is accounted for with an eddy viscosity formulation, on the basis of the following mixing length model described by the equation

$$\upsilon_T=F_1 k_{\mathrm{amb}} TI_{\mathrm{amb}}+F_2 k_2 l^{*2}\left|\frac{\partial u}{\partial r}\right|. \tag{3}$$

where $\frac{\partial u}{\partial r}$ refers to the axial velocity gradient in radial direction, k_{amb} and k_2 are DWM model constants (the k_{amb} constant includes a length scale based on a hub height equal to the rotor diameter), TI_{amb} and U_{amb} are the ambient turbulence intensity and mean wind speed at hub height, R is the rotor radius and l^* is the turbulence mixing length. F_1 and F_2 are filter functions included to govern the development of turbulent stresses. The filter functions are required, as no transport equation for turbulent kinetic energy is included in the turbulence closure of the DWM model. Without filter functions, the turbulence field would be in perfect equilibrium with the local strain-rate directly at the rotor. However, in wake modelling, the mean flow field changes abruptly at the rotor, but the process of the turbulence reaching a fully developed stage with the new local strain-rate is relatively long. The F_1 function is included to compensate for the effect on turbulence caused by the boundary condition treatment. To account for the pressure effects in the DWM model, the wake deceleration and expansion is applied at the inlet boundary (Equations (4) and (5)). This generates unphysical large velocity gradients close to the rotor. Thus, the role of the F_1 filter function is to reduce the effect of the ambient turbulence close to the rotor to avoid this unphysical turbulence diffusion of the wake deficit. Consequently, the length of the F_1 function is taken to be 2 rotor diameters (D), which is roughly equal to the distance required for the pressure to recover behind the turbine according to Sanderse.[7] The F_2 filter function governs the development of turbulence generated by the wake shear layer. This process is seen to be approximately 10 D, on the basis of AL simulations. The details and motivation for this turbulence formulation are given by Keck *et al.*[8]

The equation system described by Equations (1)−(3) is solved using a finite-difference scheme in which a second-order central-difference scheme in the radial direction and a first-order upwind scheme in the mean flow direction are applied. As information only moves along the mean flow direction, a solution can be obtained by 'marching' downstream, solving each axial position sequentially. For each location along the mean flow axis, the sequence to find the velocity field can be summarized by the following:

1. Solving the momentum equation for the streamwise velocity component at all radial positions explicitly using the value for radial velocity component and eddy viscosity from the previous location upstream. This yields a tridiagonal equation system in which all of the coefficients are known.
2. Using Equations (2) and (3) in the previous text to compute the corresponding radial velocity and the eddy viscosity (once the streamwise velocity at the present axial position is known).
3. Proceeding to the next downstream location and repeating steps 1 and 2.

1.2. The boundary condition in the DWM model

Omitting the pressure gradient term in the equations has the consequence that the near wake region, where pressure is recovering and significant gradients are present, will not be accurately represented by the DWM model. According to Sanderse,[7] this region is usually on the order of 2 D. The inaccuracy in this region is considered to be acceptable because the near wake is not of primary interest when modelling the effects of wakes on turbine operations, as long as the far-wake calculation remains accurate.

In the DWM model, the effect of the pressure gradient is considered to be negligible at a distance of 3 D behind the turbine. This location is referred to as the 'point of DWM validity'. The inlet boundary condition is designed to artificially account for the effect of the neglected pressure gradient in such a manner that the resulting flow field after 3 D is accurately represented. This is done by including expansion and deceleration of the fluid at the rotor disc. The boundary condition is based on the turbine-specific, azimuthally and time-averaged axial induction profile as a function of radial position in the rotor plane, $a(r)$. This is commonly found from an aeroelastic simulation. The pressure effects are included by scaling the turbine induction profile, both in magnitude (to account for deceleration) and the radial position where the induction is applied (to account for wake expansion), by the factors f_U and f_R, respectively. The resulting inlet velocity distribution, U_{BC}, as a function of wake radius, r_{BC}, which is applied to the DWM calculations is given by

$$U_{BC}(r_{BC}) = U_{\text{amb}}(1 - (1 + f_U)a(r)) \tag{4}$$

$$r_{BC} = r\sqrt{\frac{1-a}{1-(1+f_R)a}} \tag{5}$$

where U_{amb} is the ambient wind speed at hub height and the $\langle\rangle$ operator denotes spatial averaging over the swept rotor disc.

A least square re-calibration to CFD AL data of the model parameters and F_2 filter function was performed with the proposed modification; a description of this is given later. On the basis of the calibration, the following values were applied in the calculations: $f_U = 1.10$, $f_R = 0.98$, $k_1 = 0.587$ and $k_2 = 0.0178$. The filter functions used are shown in Figure 2.

1.3. AL model

The DWM development presented in the paper is driven by higher-order CFD predictions using AL turbine models. The fundamental processes that the proposed corrections attempt to mimic have been observed in CFD studies using the AL models, and the DWM model parameters have been calibrated against AL model calculations. The AL models used in this work are based on the formulation of Sørensen and Shen.[9] Each turbine blade is represented as a line along the blade axis, and the line is divided into a number of discrete segments. At each AL segment, a lift and drag force is calculated on the basis of the local angle of attack, chord length, actuator width and airfoil type using tabulated airfoil lift and drag properties, which are usually corrected for three-dimensional effects. These actuator forces are projected onto the CFD flow field as

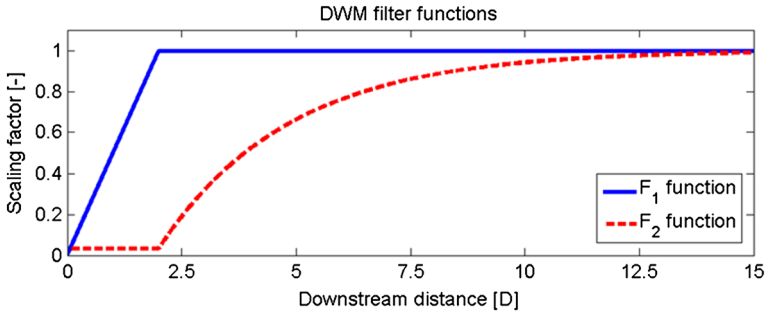

Figure 2. Filter functions applied in the DWM calculations.

volumetric body forces, in this case, using a three-dimensional Gaussian projection. The body force field enters into the N–S equations and creates the main effects of a turbine on the flow field, including axial induction, wake formation and generation of blade tip and root vortices. The main benefit of the AL model is that the high grid resolution necessary to model the boundary layer of the blades is avoided. This significantly lowers the computational expense because fewer computational cells are required, which also allows for larger time steps without violating the Courant–Friedrichs–Lewy condition.

Two different implementations of the AL model are used for DWM development and validation in this work:

- The Ellipsys3D[10] (Copenhagen, Germany) AL model developed at the Technical University of Denmark (DTU) by Mikkelsen[11] and Troldborg.[12]
- The OpenFOAM[13] implementation developed at the National Renewable Energy Laboratory by Churchfield *et al.*[14]

There are many similarities between the two implementations of the AL models. They are both incorporated into large-eddy simulation (LES) solvers and solved over relatively coarse computational grids, with a resolution such that 50–60 grid cells span the turbine rotor. LES is an unsteady CFD method that solves the filtered N–S equations, resolving the larger, energy-containing turbulent scales and modelling the effect of the remaining smaller scales.

The main difference between the models lies in the treatment of atmospheric shear and turbulence. The DTU implementation imposes a volumetric body force on the incompressible N–S equations that generates a desired atmospheric shear and turbulent fluctuations. Shear is imposed by prescribing a volume force field over the entire domain. The magnitude of the volume forces is determined through a precursor calculation in which no turbines are included, and any desired profile can be prescribed as outlined by Mikkelsen *et al.*[15] The atmospheric turbulence is imposed through fluctuating volume forces within a thin region located a few radii upstream of the wind turbine. The magnitude and fluctuations of the volume forces are based on a pre-generated turbulence field, which is translated into a force field by the one-dimensional momentum theory, as described by Troldborg *et al.*[16] Keck *et al.*[17] validated this method for simulations of a wind turbine wake, represented by the EllipSys3D AL model, in natural atmospheric turbulence to field and wind tunnel data. The validation campaign comprised of validation of the evolution of turbulence intensity, turbulence spectra and wake meandering as a function of downstream distance for a range of common operating conditions.

The National Renewable Energy Laboratory implementation also solves the incompressible N–S equation for motion, but thermal effects are accounted for through a Boussinesq buoyancy term. This term allows for the modelling of atmospheric stability (in this work, however, all simulations were carried out in neutral stratification). Rather than using a force field to create the atmospheric shear and turbulence, these effects are generated by running precursor atmospheric boundary layer (ABL) calculations in a horizontally periodic turbine-free domain. After the turbulent boundary layer has developed to a quasi-equilibrium state, velocity and temperature information at the upstream boundaries are stored at every time step. This data is then used in the turbine simulations as time-dependent inlet boundary conditions. The benefit over the DTU implementation is that the shear and turbulence used for the wind turbine simulation are generated directly from the N–S equations and that buoyancy effects on the turbulence production can be captured. The disadvantage is that the method is significantly more computationally expensive. The details of this method are outlined by Churchfield *et al.*[14]

Figure 3 shows a comparison of the input turbulence spectra in neutral stratification to the EllipSys3D AL model [prescribed by the Mann model (Mann[18] and[19]), thick lines], to that of the OpenFOAM AL model (generated by the precursor, thin lines). The input turbulence spectra of the normal stress components are in fair agreement for all scales

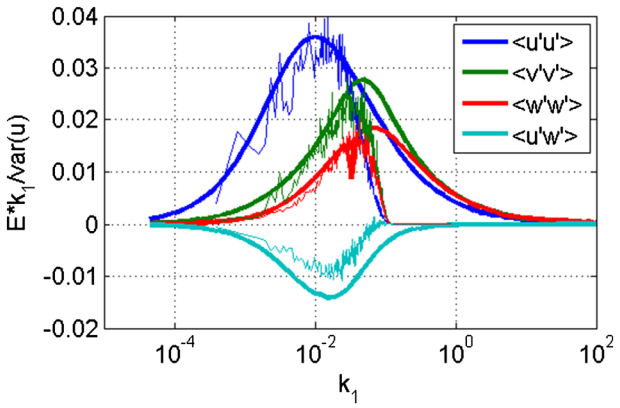

Figure 3. Turbulent energy spectra of the input wind field to the EllipSys3D AL model (thick lines) and the OpenFOAM AL model (thin lines).

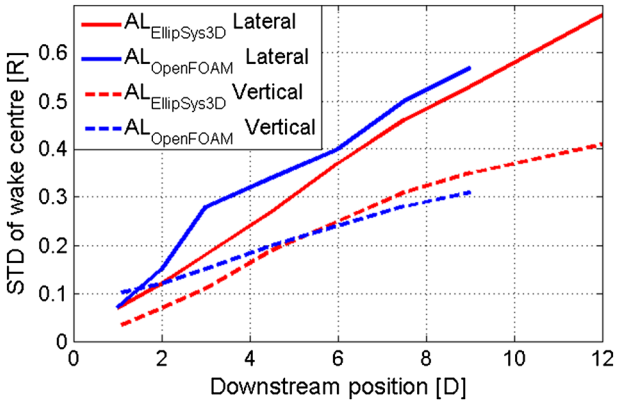

Figure 4. Wake meandering downstream of a single turbine operating in 8 m s^{-1} wind speed and 6% as modelled by the EllipSys3D AL model (red lines) and OpenFOAM AL model (blue lines). The wake meandering is quantified as the standard deviation of the wake centre and normalized against rotor radius.

above the spectral cut-off due to the grid size of the LES precursor calculations. The largest deviation is seen for the shear stress component (cyan line), which is lower in the OpenFOAM precursor compared with that of the Mann model.

Figure 4 shows the wake meandering resulting from the two models for a single turbine with a rotor diameter of 80 m, represented as ALs, operating in 8 m s^{-1} wind speed and 6% turbulence intensity. The wake meandering is quantified as the standard deviation of the wake centre. The method selected to find the wake centre in the two models is slightly different because of the availability of data. In this work, the EllipSys3D AL simulations are setup to allow for analysis in the MFoR (i.e. in a coordinate system following the centre of the wake, which allows for studies of the wake deficit evolution). This requires storing planes of data in whole cross sections of the wake and calculating the wake centre as the centre of gravity of the wake deficit at each time step. This procedure to find the wake centre in the EllipSys3D simulations is described in Keck *et al.*[17] The OpenFOAM calculations are setup to be used as validation of the DWM model in the fixed frame of reference (FFoR, i.e. relative to a fixed location and therefore affected by both wake deficit evolution and wake meandering). To facilitate an analysis in the FFoR, data was stored in a lateral plane and in a vertical plane, with a joint axis aligned with the mean wake axis (i.e. the axis extending into the wake from the hub of the wind turbine in the mean wind direction). The wake centre position is found as the location where a simplified wake shape gives the best fit with the instantaneous wake deficit (see Keck *et al.*[20] for more details). The first algorithm has higher accuracy but increases the amount of data that needs to be stored by an order of magnitude, and the analysis to find the wake centre is more time consuming, relative to the second algorithm. Since it is not critical to the analysis of this study to accurately quantify the wake meandering of the OpenFOAM AL simulations (we are only interested in the resulting flow field at hub height), the inexpensive second algorithm is applied to the OpenFOAM simulations. From Figure 4, it is seen that the two models yield similar magnitude of wake meandering in both lateral (solid lines) and vertical (dashed lines) directions. This is expected as the input turbulence spectra in Figure 3 are in fair agreement in large scales, which dictates the meandering.

1.4. Atmospheric shear contribution to turbulence in the DWM deficit model

In the DWM model, the turbulent stresses are calculated on the basis of the zero-equation eddy viscosity model shown in Equation (3). In a zero-equation eddy viscosity model, there is no transport equation for turbulent kinetic energy to maintain an integrated balance of production and dissipation. Instead, the eddy viscosity is directly proportional to the local mean flow gradients. Further, in all eddy viscosity models, the turbulent stresses are calculated as the product of the eddy viscosity and the local velocity gradients. As a consequence, it is very important for the calculation of the turbulent stresses to apply the correct total mean velocity gradient in the model.

In the current formulation, only the wake deficit gradient is considered when calculating the turbulent stresses in the DWM model. This limitation has the undesirable effect that, as the wake deficit recovers, the turbulent stresses approach zero, resulting in unrealistically low turbulent stress levels in the far-wake region. An appropriate turbulence formulation should result in ambient turbulence conditions after the wake deficit has fully recovered. The proposed method is to include a strain-rate contribution from the atmospheric vertical wind shear when calculating the turbulent stresses. A difficulty, though, is that atmospheric shear is not axisymmetric but the DWM model wake deficit formulation is.

The magnitude of the atmospheric shear gradient should be expressed as a function of ambient turbulence intensity to fit with the existing DWM input parameters. An appropriate dimensionless wind shear value can be found by estimating

the non-dimensional characteristic velocity and length scale, u^*_{ABL} and l^*_{ABL}, of the atmospheric turbulence and using the relation

$$\frac{du}{dz_{ABL}} = \frac{u^*_{ABL}}{l^*_{ABL}}. \tag{6}$$

The velocity scale is based on the neutral atmospheric turbulence spectra, as calculated by the model proposed by Mann.[18,19] To be compatible with the DWM model parameters, the atmospheric velocity scale is formulated as a function of ambient turbulence intensity. This is achieved by relating the normal stresses (given by the turbulence intensity level) to the shear stresses in the atmosphere (which yield the velocity scale) through integration of the turbulent energy in the atmospheric turbulence spectra,

$$u^*_{ABL} = \left[\left(TI^2_{\text{amb}} \cdot \frac{-\overline{u'w'}}{\overline{u'u'}}\right)\right]^{1/2} \tag{7}$$

where TI_{amb} is the ambient turbulent intensity and $\overline{u'u'}$ and $-\overline{u'w'}$ are the normal and shear stresses of the atmospheric turbulence, respectively. The overbar denotes time averaging. The atmospheric length scale is estimated using Monin–Obukhov scaling given by Ratto,[21]

$$l^*_{ABL} = \frac{\kappa z}{R} \tag{8}$$

where κ is the von Kármán constant, z is the height above the ground level and R is the rotor radius. This atmospheric shear is calculated at a reference height of 100 m, and it is considered to be linear and have one uniform value in the whole simulation domain (i.e. it is invariant in downstream direction and height). Further, it is also assumed to be unaffected by the presence of the wake deficit. The effect of the atmospheric shear is to increase the local strain-rate and, thereby, the turbulent stresses in regions of low wake deficit gradients. This is typically the far-wake region but also may include the regions close to the wake centreline and the rotor for nearly uniform induction profiles.

The strain-rate to apply in the DWM calculations should be a function of radial and axial positions, where each value corresponds to the azimuthally averaged axial velocity gradient with respect to radial direction (as the deficit is based on two-dimensional calculation, variations in azimuthal directions cannot be captured). As the atmospheric shear is expressed in Cartesian coordinates (du/dz) and the wake deficit gradient is in axisymmetric coordinates (du/dr), an appropriate method is required to combine the two gradients to find the representative strain-rate. To illustrate the proposed method, the local radial gradient of axial velocity of the two velocity gradients is drawn as a function of azimuthal position for some arbitrary radial location in the wake deficit in Figure 5. The wake deficit gradient (dashed lines) has a constant value as a function of azimuthal position, as the DWM model assumes axisymmetric flow. The contribution due to the atmospheric shear gradient (dotted lines) is a sinusoidal function over the azimuth, as linear atmospheric shear is assumed over the cross section of the rotor. The combined local gradient (solid line) is the sum of the two contributions. Since the deficit calculation in the DWM

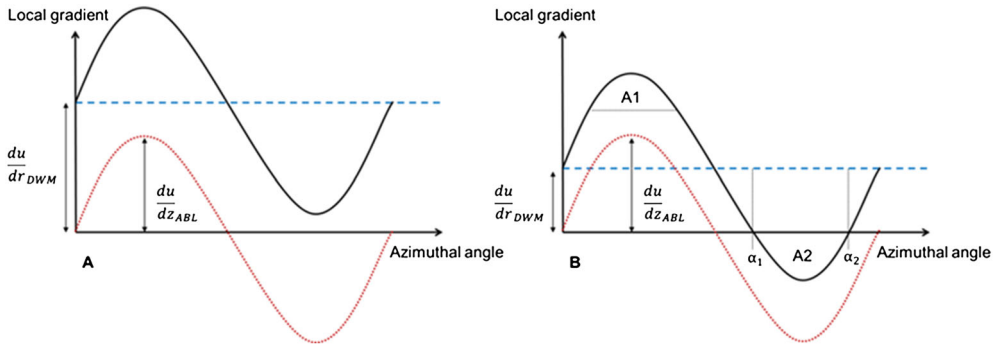

Figure 5. Conceptual description of how the local representative velocity gradient (solid line) is calculated given the atmospheric shear (dotted line) in Cartesian coordinates (du/dz) and the wake deficit gradient (dashed line in axisymmetric coordinates (du/dr).Figure 5(a) (left) illustrates a case in which the magnitude of the wake deficit shear is larger than the atmospheric shear, and Figure 5(b) (right) illustrates a case in which the atmospheric shear is larger.

model assumes an axisymmetric flow field, the representative value for the strain-rate to apply is the mean value in azimuthal direction. This value corresponds to the average height of the combined curve in Figure 5.

An important observation is that when the magnitude of the wake-deficit gradient is larger than the atmospheric shear, the mean effect of the atmospheric gradient is zero, as shown in Figure 5(a). This is the same as saying that the integral of the total local gradient is equal to the integral of constant wake deficit gradients. In this region, no correction due to atmospheric shear is required. The correction should therefore only give a non-zero contribution when the magnitude of the atmospheric shear gradient is larger than the wake deficit gradient.

When the magnitude of the atmospheric shear is larger than the wake deficit gradient, a part of the lower wake (*A2* in Figure 5(b)) will experience turbulent stresses acting in the opposite direction compared with the rest of the wake. Since the DWM model is based on an axisymmetric flow field, this situation cannot be handled in a strictly physically manner. Instead, the key feature to capture for the wake diffusion is the total magnitude of turbulent stresses. This magnitude is found by calculating the azimuthal average of the absolute value of local velocity gradient at each radial position. This gradient is then used to calculate the turbulent stresses. The geometrical interpretation of this concept is that the representative strain-rate to apply in the stress calculations corresponds to the average (absolute) distance between the combined curve and the *x*-axis in Figure 5(b). The representative strain-rate can thus be calculated using the equations

$$A_{\text{Total}} = \begin{cases} 2\pi \dfrac{du}{dr_{DWM}} & , \quad \left|\dfrac{du}{dr_{DWM}}\right| \geq \dfrac{du}{dz_{ABL}} \\ 2\pi \dfrac{du}{dr_{DWM}} + A1 + A2, & \left|\dfrac{du}{dr_{DWM}}\right| < \dfrac{du}{dz_{ABL}} \end{cases} \tag{9}$$

$$A1 = A2 = \int_{\alpha_1}^{\alpha_2} \left(\frac{du}{dz_{ABL}} \cdot \sin(x) dx \right) - (\alpha_2 - \alpha_1) \frac{du}{dr_{DWM}} \tag{10}$$

$$\frac{du}{dr_{\text{Total}}} = \frac{A_{\text{Total}}}{2\pi} \tag{11}$$

For a given radial position, the azimuthal section of the deficit in which the atmospheric shear contribution is larger than the wake deficit shear, i.e. between α_1 and α_2, are found by $arcsin\left(\frac{du}{dr_{DWM}} \Big/ \frac{du}{dz_{ABL}}\right)$ and π-α_1, respectively. The strain-rate, as calculated by Equation (11), is used to calculate the turbulent stresses in the wake to incorporate the effect of the atmospheric shear on the wake diffusion. Rather than using the total velocity gradient in the turbulent stress term of the momentum equation, Equation (1), and because the momentum equation is only meant to solve for wake velocity and not a combined wake-atmospheric velocity, a scaled eddy viscosity, ν_t', is introduced as

$$\nu_t' = \nu_t \cdot \frac{\frac{du}{dr\text{Total}}}{\left|\frac{du}{dr DWM}\right|}. \tag{12}$$

The original eddy viscosity is scaled at every computational node by the ratio of the corrected gradient with atmospheric shear effects to the wake deficit velocity gradient in the DWM solution. This has the desired effect of applying the appropriately scaled turbulent stresses, τ, in the wake deficit calculation

$$\tau = \nu_t' \cdot \frac{du}{dr_{DWM}} = \nu_t \cdot \frac{\frac{du}{dr\text{Total}}}{\left|\frac{du}{dr_{DWM}}\right|} \cdot \frac{du}{dr_{DWM}} = \nu_t \cdot \frac{du}{dr_{\text{Total}}} \tag{13}$$

A correction is included to ensure numerical stability in regions with wake deficit velocity gradients close to zero. Because the total mean velocity gradient according Equation (11) never approaches zero, numerical instabilities occur in the scaling of the eddy viscosity, as the last term of Equation (12) approaches infinity. This is solved by the application of a Wiener filter,[22]

$$\frac{1}{\frac{du}{dr_{DWM}}} \approx \frac{\frac{du}{dr_{DWM}}}{\left(\frac{du^2}{dr_{DWM}} + k_{\text{wiener}}\right)} \tag{14}$$

where $\frac{du}{dr_{DWM}}$ is the azimuthally average wake deficit gradient and k_{wiener} is the Wiener constant. The value of the Wiener constant is selected on the basis of the size of the atmospheric shear and the radial resolution of the DWM model, Δr_{DWM}. These

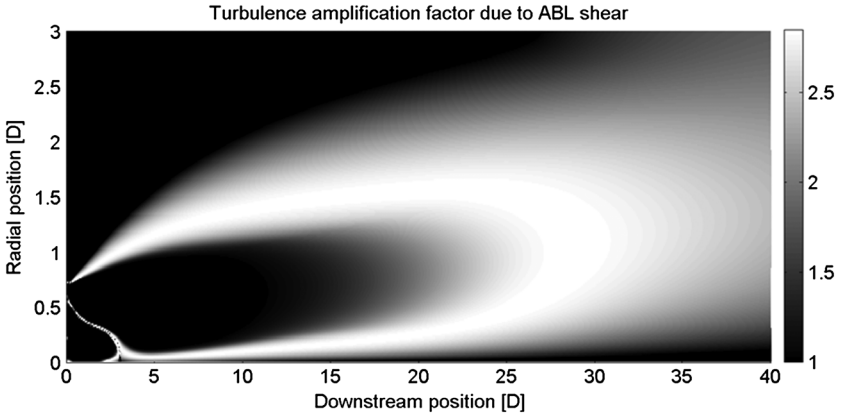

Figure 6. The local amplification of turbulent stresses caused by the atmospheric shear contribution, given by the second term of Equation (12) (i.e. $\frac{du}{dr}_{\text{Total}} / \left|\frac{du}{dr}_{DWM}\right|$), as a function of radial and downstream position. The *x*-axis of the figure lies on the centreline of the wake. The ambient wind speed for the displayed case is 8 m s^{-1}, and the turbulence intensity is 14%.

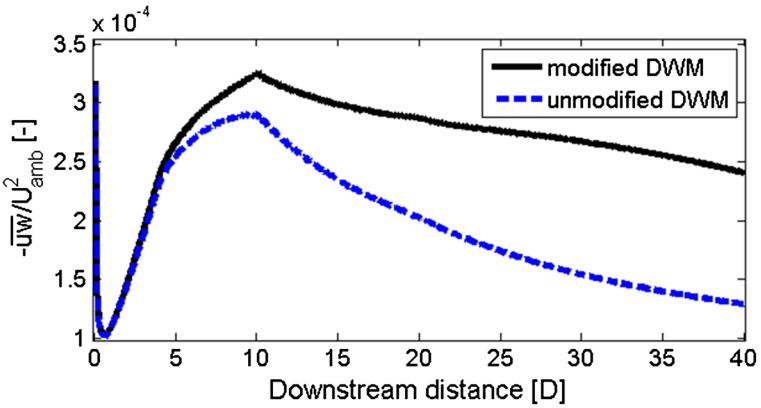

Figure 7. The normalized turbulent shear stress level, spatially averaged over the wake from the centre of the wake to 3 D in radial direction, as found by the unmodified DWM model (dashed blue line)and the shear corrected DWM model (solid black line)as a function of downstream position. The overbar operator refers to time averaging for the Reynolds stresses.

properties are used to define the constant as they represent the magnitude of the nominator and the discretization error of the wake deficit gradient, which both influence the sensitivity of the eddy viscosity scaling factor

$$k_{\text{wiener}} = 2\frac{du}{dz_{ABL}} \cdot \Delta r_{DWM}^2 \cdot \tag{15}$$

The effect of the proposed corrections on wake turbulence in a simulation run with a wind speed of 8 m s^{-1}, and a turbulence intensity of 14% is shown in Figures 6 and 7. Figure 6 shows the local amplification of the turbulent stress given by second term of Equation (13). As previously described, the turbulent stresses are not scaled at locations where the wake deficit gradients are larger than the atmospheric gradient. This is shown in the figure by the dark core in the majority of the wake region for the first 12 D downstream of the rotor. The atmospheric shear correction influences the turbulent stresses close to the centre axis of the wake and outside the wake shear layer relatively close to the rotor. As the wake deficit recovers and the strain-rate caused by the wake is reduced, an effect on the turbulent stresses near occurs throughout the whole wake deficit. The effect of the atmospheric shear correction on the turbulent stresses is shown in Figure 7. The averaging is carried out from the centre of the wake to 3 D in radial direction. The effect of atmospheric shear on the turbulence level is small over the first 5 D downstream of the turbine. At 5 D, it starts to increase, reaching about 30% to 100% higher average turbulent stress levels in the region from 15 D to 40 D.

The computational time to find the wake deficit in the DWM model increases by ~15% by including the atmospheric shear contribution, from 2.25 to 2.64 s, when calculating the flow field over the first 15 D on a standard laptop. As the

DWM model is designed to be used with aeroelastic software, this increase in computational time is negligible compared with the time consumed by the aeroelastic software.

1.5. DWM calibration

After the atmospheric shear contribution to the turbulence stresses is implemented in the DWM model, a re-calibration is required. This re-calibration ensures that the newly implemented correction actually provides a better fit to higher-order CFD AL models (i.e. that more physics is captured) and to find the appropriate values for the model coefficients and the upstream boundary condition scaling parameters. The basis of the calibration is to minimize the average standard error (STE) of the DWM flow field compared with results extracted from Ellipsys3D AL simulations. The reason that the DWM model is calibrated to the EllipSys3D AL results, and not the OpenFOAM AL model, is that data from the EllipSys3D AL simulations are available in planes covering the whole cross section of the wake. Having planes of the data covering the wake cross section enables calibration of the wake deficit formulation in the DWM model to be conducted in the MFoR, thus removing the influence of wake meandering. This procedure is described in Keck *et al.*[17] The STE is defined as the standard deviation in mean velocity between the AL and the DWM models

$$\mathrm{STE} = \sqrt{\frac{1}{n_c}\sum_{c=1}^{n_c}\left[\frac{1}{n_{c,d}}\sum_{d=1}^{n_d}\left(\frac{1}{n_{c,d,r}}\sum_{r=1}^{n_{c,d,r}}\left(\overline{U}_{c,d,r}^{ACL}-\overline{U}_{c,d,r}^{DWM}\right)^2\right)\right]} \tag{16}$$

where the indexes c, d and r correspond to cases (i.e. variations in inflow conditions), downstream distance and radial position, respectively. The constants, n_c, $n_{c,d}$ and $n_{c,d,r}$, represent the number of cases, number of cross sections and number of data points per cross section, respectively. In this calibration, the constants are equal to six flow cases (wind speeds of 6 and 10 m s^{-1}, turbulence intensities of 6%, 10% and 14%), five cross sections for each case (3, 4.5, 6, 7.5 and 9 D behind the rotor) and 80 points per cross section (radial coordinates from the rotor centre to 1.6 R). The calibration is carried out in three steps, all based on the gradient-based simplex method of Lagarias *et al.*,[23] which is also outlined in the MATLAB user guide.[24]

Step 1. **Calibrate the boundary condition**

The DWM inlet boundary condition is calibrated to yield a velocity field as close as possible to the Ellipsys3D AL mean velocity field at 3 D behind the rotor. As discussed earlier, this is necessary in order to account for the effects of the omitted pressure gradient on the wake deficit development in the DWM model. The pressure gradient effects (expanding and reducing the velocity of the initial deficit caused by turbine induction) are captured by the scaled inlet boundary condition. The boundary condition is, therefore, a function of four model parameters: the inlet deficit modification parameters f_U and f_R, along with the eddy viscosity constants and the filter functions from 0 to 3 D, $k_1{*}F_{1,\ 0\text{–}3D}$ and $k_2{*}F_{2,\ 0\text{–}3D}$.

Step 2. **Calibrate filter functions F_2**

The F_2 filter function is included in the DWM model to govern the development of turbulence generated by the wake shear layer. Such a function is required, as the turbulence closure of the DWM model is a zero-equation eddy viscosity model. Because no transport equation is modelled, the turbulence is calculated on the basis of the local mean flow gradient. The mean flow field over the rotor changes very abruptly, and steep mean flow gradients are created very close to the turbine. The turbulence, on the other hand, requires distance to reach equilibrium with the mean flow. In many cases, this is on the order of 6–10 D downstream of the turbine. This effect is captured by the F_2 function. The F_1 function is related to the treatment of the pressure field in the boundary conditions of the DWM model. The pressure field recovers in the first two rotor diameters downstream of the turbine. Therefore, no additional calibration is made to the F_1 function (Equation (17)), which is assumed to follow the suggestion given in Madsen *et al.*[1]

The F_2 filter function is found by using the k_1, the f_U and f_R parameters from step 1 and running the simplex optimization to find the optimum value of $k_2{*}F_2$ at different downstream positions. The calibration is performed at 3, 4.5, 6, 7.5 and 9 D against single Ellipsys3D AL mean velocity cross sections. This yields the optimum value of $k_2{*}F_2$ at five locations in the wake. Since it is desired to have a smoothly increasing filter function that reaches unity in the far-wake, an F_2 filter function is constructed by fitting an exponential saturation function through the five points. The applied filter functions are given by Equations (17) and (18), respectively, where x refers to the downstream position expressed in rotor diameters relative to the wake emitting turbine. The F_1 filter function varies linearly from 0 to 1 over the first two diameters of flow to compensate for the boundary conditions treatment of the DWM model. The F_2 filter function

consists of two parts; the first part is related to the boundary condition treatment and the second part to the development of shear layer generated turbulence in the wake.

$$F_1 = \begin{cases} x/2 & x < 2D \\ 1 & x > 2D \end{cases} \tag{17}$$

$$F_2 = \begin{cases} 0.035 & x < 2D \\ 1 - 0.965e^{-0.35(x-2)} & x > 2D \end{cases} \tag{18}$$

Step 3. **Global calibration of k_1, k_2, f_U and f_R**

In this step, simplex optimization is performed on the four model parameters using the entire Ellipsys3D AL dataset with all cases and all cross sections and also using the filter function found in step 2. The values k_1, k_2, f_U and f_R found previously are used as initial conditions to the optimization algorithm. This step fine tunes these model parameters.

The STE with the atmospheric shear contribution to turbulence included is 5.3% smaller than for the existing DWM model, which is reduced from 0.017 to 0.016. This reduction is an indication that the atmospheric shear contribution does capture a relevant physical process of the wake dynamics and recovery.

1.6. Improved wake-added turbulence formulation

After including the contribution of the atmospheric shear gradient in the calculation of the turbulent shear stresses in the DWM deficit calculations, the far-wake stresses are maintained at realistic levels. This makes it is possible to formulate an expression for wake-added turbulence, which is consistent with the simplified N–S solution that governs the velocity deficit. We propose that after including the correction for atmospheric turbulence, the wake-added turbulence at a downstream rotor should be based on turbulent shear stresses used in the wake deficit calculations of the upstream, oncoming wake. This would result in a more realistic build-up of turbulence intensity over a row of turbines, compared with using the ambient turbulence intensity level to prescribe the wake evolution, as is the current standard method. The most straightforward method for coupling the wake turbulence of the upstream rotor to the inflow of the downstream rotor is through the turbulence stresses of the oncoming wake. This requires the turbulent stresses in the deficit calculation to be expressed as a local estimation of the turbulence intensity before being applied in the DWM calculations for the next rotor. This can be achieved by approximating the turbulent stresses in the normal direction based on the turbulent shear stresses using the relation,

$$-\overline{u'w'} = u'_{rms} w'_{rms} \cdot Cu'w' \tag{19}$$

where $C_{u'w'}$ is the correlation coefficient between axial and radial velocity fluctuations and u' and w' are the axial and radial fluctuations in the wake, respectively. The overbar denotes time averaging, and the subscript *rms* refers to the root-mean-square of the fluctuating components over time. Rewriting the radial velocity fluctuations as,

$$w'_{rms} = \frac{w'_{rms}}{u'_{rms}} u'_{rms} \tag{20}$$

inserting Equation (20) into Equation (19) and rearranging the terms yields,

$$-\overline{u'w'} = u'_{rms} \cdot u'_{rms} \frac{w'_{rms}}{u'_{rms}} \cdot C_{u'w'}. \tag{21}$$

By using the fact that the axial fluctuations are perfectly correlated with themselves (i.e. $u'_{rms} u'_{rms} = \overline{u'u'}$), Equation (21) can be arranged to estimate the streamwise component of the Reynolds stress as

$$\overline{u'u'} = \frac{1}{C_{u'w'} \cdot \left(w'_{rms}/u'_{rms}\right)} \cdot - \overline{u'w'}. \tag{22}$$

The correlation coefficient, $C_{u'w'}$, and the $\frac{w'_{rms}}{u'_{rms}}$ ratio of wake generated turbulence is different compared with atmospheric turbulence because of the higher degree of isotropy and short turbulent length scale. In this work, these properties have been

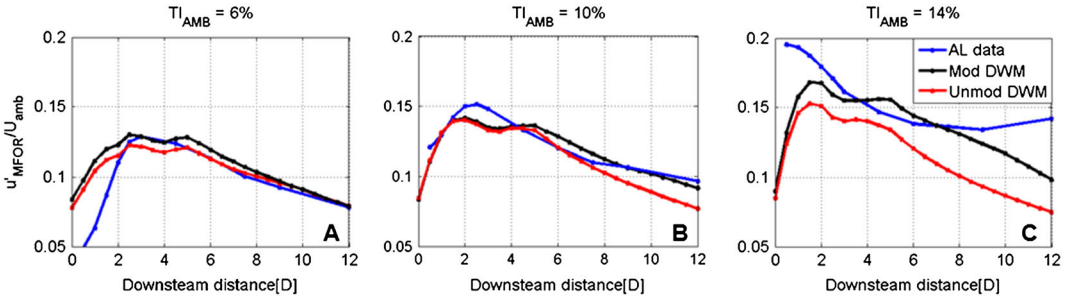

Figure 8. The effect of the atmospheric shear correction on the mean turbulence intensity of wake in the MFoR as a function of downstream distance from the wake-emitting turbine and ambient turbulence intensity. The wake turbulence evolution of the DWM models is compared with that of the EllipSys3D AL model for a turbine operating in ambient turbulence intensities of 6% (A), 10% (B) and 14% (C).

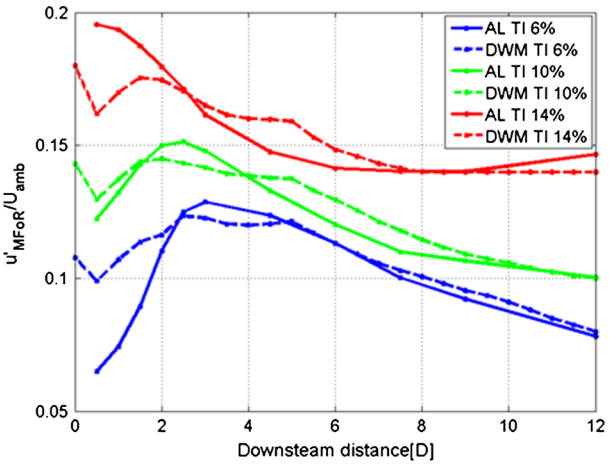

Figure 9. The DWM (dashed lines) and the Ellipsys3D AL (solid lines) model-predicted turbulence intensity in the MFoR as a function of downstream distance from the wind turbine.

given the values of 0.3 and unity, respectively, on the basis of the findings of Larsen *et al.*[25] Inserting the dimensionless DWM shear stresses into Equation (22) and taking the square root yields an approximation of the turbulence intensity in the DWM model [left term under the max-operator in Equation (23)]. As the output of Equation (23) will be used to estimate the turbulence at downstream rotors in an FFoR, a correction is included to ensure that the turbulence intensity in the wake region always assumes a value that is equal or greater than the ambient turbulence intensity (TI_{amb}). This correction is required for two reasons: (i) to remove regions of low turbulence in the wake deficit (these exist at the wake axis because of symmetry effects on the mean gradient) and (ii) to set the ambient turbulence value at all computational nodes outside of the wake deficit (where the deficit model does not contain any turbulent stresses) before adding the effect of wake meandering to find the turbulence at a downstream turbine. The effect of this correction can be seen in Figures 8 and 9.

$$TI_{DWM\ MFoR} = \max\left(\sqrt{\frac{1}{C_{u'w'}\cdot\left(w'_{rms}/u'_{rms}\right)}\cdot\tau_{\text{stress DWM}}}, TI_{amb}\right). \tag{23}$$

Equation (23) yields a local value of wake turbulence intensity for each computational node in the DWM domain, $TI_{DWM\ MFoR}$. The DWM deficit module outputs the wind speed (Equation (1)) and turbulence distribution (Equation (23)) in the MFoR (i.e. without any large-scale movements). The meandering can be viewed as a series of wake segments in which the wake centre has a stochastic offset in lateral and vertical direction according to some statistical distribution. If this distribution of the meandering is known, it is possible to calculate the average wind field and turbulence intensity at the downstream rotor by calculating the convolution between the deficit [both wind speed and variance, i.e. the square of $TI_{DWM\ MFoR}$

from Equation (23)] in MFoR and the distribution of the wake centre in the vertical and lateral direction because of wake meandering as follows

$$\theta_{DWM\ FFoR} = \iint \theta(y - y_m, z - z_m)_{DWM\ MFoR} \cdot PDF_m(y_m, z_m) dy_m dz_m. \tag{24}$$

In this equation, θ represents the wind speed or variance distribution in the MFoR; $y-y_m$ and $z-z_m$ are the local coordinates in the MFoR; and PDF_m is the probability density function for the meandering distribution. In this work, a Gaussian distribution is used to describe the meandering of the wake deficit. The standard deviation of the wake deficit location in lateral and vertical directions is extracted from Ellipsys3D AL calculations, where the wake centre is taken to be the centre of gravity of the wake deficit in a plane perpendicular to the mean flow. The subscripts *FFoR* and *MFoR* refer to the fixed and MFoR. Equation (24) results in a wind speed and variance distribution in FFoR.

Using the DWM model to conduct simulations over a row of wind turbines, the flow field in FFoR is used to find the turbulence intensity and velocity distributions to apply as 'ambient conditions' at the downstream rotor. However, as the deficit calculation of the DWM model is based on an axisymmetric formulation, the flow field in FFoR needs to be transformed using Equations (25) and (26) before it can be applied as boundary conditions at the subsequent rotor. The input velocity field to the wake-affected turbine is a function of radial coordinate (r), whereas the input turbulence intensity is a single number representing the mean value over a cross section of the wake (because of the eddy viscosity model, it is non-trivial to couple the turbulence distribution in the oncoming wake to the subsequent wake deficit evolution).

$$U_{\text{axisym}}(r) = \frac{1}{2\pi\Delta r} \int_0^{2\pi} \int_{r-\frac{\Delta r}{2}}^{r+\frac{\Delta r}{2}} U_{DWM\ FFoR}(y_{WTG} + r\cos(\alpha), z_{WTG} + r\sin(\alpha))\ dr\ d\alpha \tag{25}$$

$$TI_{WTG} = \frac{1}{2\pi R_w} \sqrt{\int_0^{2\pi} \int_o^{R_w} TI^2_{DWM\ FFoR}(y_{WTG} + r\cos(\alpha), z_{WTG} + r\sin(\alpha))\ dr\ d\alpha} \tag{26}$$

R_w is the initial width of the wake deficit in the DWM model and is calculated by Equation (5) by applying the rotor radius as r value. The mean turbulence intensity level given by Equation (26) represents the mean turbulence intensity in the scales that affect the wake deficit evolution (roughly corresponding to eddies smaller than 2 D, according to Larsen *et al.*[4]). This is, therefore, the appropriate value to use when coupling the turbulence intensity of the wake to the downstream evolution of the wake-affected wind turbine. However, to find the total turbulence intensity at the downstream turbine (in FFoR), which is relevant to loads or when comparing with reference data, a contribution that is caused by the meandering of the mean velocity deficit needs to be included. This is referred to as the 'apparent turbulence intensity',

$$TI_M(y, z) = \sqrt{\iint \left(U(y - y_m, z - z_m)_{MFoR} - U_{FFoR}(y, z)\right)^2 \cdot PDF_m(y_m, z_m) dy_m dz_m} \tag{27}$$

where the first term can be thought of as the distribution of wind speeds at location 'y, z' because of the meandering deficit, and the second term represents the mean wind speed in FFoR. The contribution of Equations (24) and (27) can be considered as independent because of the split in scales, which means that the total turbulence intensity in FFoR can be found by Equation (24):

$$TI_{tot\ FFoR} = \sqrt{TI_M^2 + TI^2_{DWM\ FFoR}}. \tag{28}$$

1.7. A method for applying the DWM model to a row of wind turbines

An investigation using the DWM model, including the new formulation for atmospheric shear contribution and wake-added turbulence, was conducted for a case of eight turbines aligned with the wind direction. The goal of the investigation was to quantify the effect of the DWM model improvements on the power prediction along a row of turbines.

The first rotor experiences the ambient wind speed and turbulence intensity. For the downstream turbines, new inflow conditions need to be calculated using Equation (24–26) and will include the wake deficit, wake meandering and an increased small-scale turbulence level. The resulting inflow conditions will be a function of the upstream turbine's operational characteristics, the ambient conditions and the distance between the turbines.

The mean wind speed and turbulence intensity, Equations (25) and (26), are used to find the appropriate induction and turbulent mixing in the eddy viscosity model for the downstream rotors. The mean wind speed as a function of radial position, given by Equation (25), is also used to keep track of the mean flow field over the entire row of turbines. The induction of the turbine [including the scaling of the deficit by f_U and f_R according to the DWM boundary condition according to Equations (4) and (5)] is linearly superimposed onto the oncoming averaged wind field. The resulting flow field is used as the inlet boundary condition in the DWM model deficit calculation and is thus a combination of the incoming non-uniform wind and turbine induction. The same procedure is used at the subsequent rotors in the row.

Using this method, both the reduction in mean wind and the increase in turbulence intensity are being built up over the row of turbines. It is, however, assumed that the scale of the increased turbulence in the wake deficit is sufficiently small to avoid affecting the large-scale wake meandering. Therefore, the meandering statistics are not changed over the row of turbines and are maintained on the basis of the larger scale fluctuations in the ambient winds for all turbines in the row.

The implementation of the DWM model used to investigate the effects of the atmospheric shear contribution to turbulence and the build-up of turbulence over a row of turbines is not coupled to an aeroelastic software. Therefore, power is estimated directly from the oncoming flow field. Because the instantaneous power production is a function of the cube of the local wind speed (below rated power), the time averaged wind speed field cannot be used directly for power estimations. To account for dynamic effects on power production due to partial wake operations caused by meandering, or the wind direction not being perpendicular to the row of turbines, a separate velocity field for power estimation is calculated using the equation

$$U_{\text{power } FFoR} = \sqrt[3]{\iint U^3(y - y_m, z - z_m)_{DWM\ MFoR} \cdot PDF_m(y_m, z_m) dy_m dz_m}, \tag{29}$$

where, again, $y-y_m$ and $z-z_m$ are the local coordinates in the MFoR and PDF_m is the probability density function for the meandering distribution. $U_{\text{power } FFoR}$ is the cube root of the mean value of the cube of the wind speed field in the FFoR. When this quantity is applied for power estimation, the effect that instantaneous power production is based on the local wind speed to the power of three is captured. By applying $U_{\text{power } FFoR}$ in Equation (25), an expression for the velocity field for power estimation as a function of radial position, $U_{\text{power}}(r)$, is found. The power production of the turbines may then be estimated using the equation,

$$P_{WTG} = \int_0^R \left[\left(4a(r) \cdot (1 - a(r))^2 \right) \cdot \frac{1}{2} U^2_{\text{power}}(r) \cdot U_{\text{power}}(r)\ 2\pi r\ dr \right] \cdot f_{mek} \tag{30}$$

where $a(r)$ is the azimuthally averaged rotor induction. The first term under the integration is an estimation of the coefficient of power, C_p, followed by the kinetic energy per unit mass at the rotor, mass flow and a factor for system losses from mechanical power to electricity (f_{mek} is estimated to be 0.9). Note that $a(r)$ refers to the average turbine induction and is not scaled by f_U and f_R, as in the DWM model boundary condition.

2. RESULTS AND DISCUSSION

2.1. Validation of wake turbulence on the basis of the DWM model-predicted Reynolds stress

The method described by Equations (19–23) for estimating the turbulence intensity in the wake of the DWM model on the basis of the turbulent stresses is validated by comparing the mean turbulence intensity in the wake as a function of downstream distance to the Ellpisys3D AL model calculations of Keck *et al.*[17] Because the DWM model deficit equation is designed to handle the wake deficit development without meandering, it is compared with AL data in the MFoR (i.e. following the centre position of the wake deficit).

In the first analysis, the turbulence intensity found by Equation (23) was investigated without including the correction to ensure that the local turbulence intensity is always equal to or larger than the ambient turbulence intensity [i.e. using only the left term under the max operator of Equation (23)]. This term represents the turbulent stresses that act on the wake deficit in the DWM model. The results in Figure 8 show the mean turbulence intensity over a cross section of the wake as a function of downstream distance.

Figure 8 shows the effect of including the ABL shear contribution in the eddy viscosity calculation of the DWM wake deficit for three different ambient turbulence intensities: 6% (A), 10% (B) and 14% (C). All cases conducted for a single wind turbine with a rotor diameter of 80 m, operating in neutral stratification with a mean wind speed of 8 m s^{-1}. The figure shows that the inclusion of the ABL shear contribution results in a higher mean turbulence level in the wake of the DWM model, relative to the unmodified DWM model. The effect is larger for higher turbulence intensity as the ABL shear gradient increases with turbulence intensity under neutral stratification. Compared with the unmodified DWM version, the turbulence predictions of the modified DWM model agree better with the AL reference data. The largest improvements are seen in the far-wake region (where the wake deficit shear is small), and the effect increases with increasing ambient turbulence intensity (as the ABL shear increases). The modified DWM model slightly overpredicts the turbulence intensity between 4 and 6 D behind the rotor. The over-prediction is on the order of 0.5–1.0 percentage points (pp, i.e. ΔTI). The far-wake turbulence agrees well for the 6% and 10% cases (A and B) but is under-predicted for the 14% case (C). At 10–12 D, the turbulence intensity of the 14% case is under-predicted by ~2.5 pp.

As mentioned earlier, before coupling the turbulence intensity estimation to calculate the average turbulence intensity at the downstream turbine, the low turbulence regions are corrected by the ambient turbulence intensity [right term of Equation (23)]. These low turbulence intensity regions in the DWM model exist at a location where the velocity gradient of the deficit is close to zero. The turbulence in these regions will become low as there is no transport equation for turbulent stresses in the DWM model, and the ABL shear correction will not have full effect because of a Wiener filter (included for numerical stability). To avoid having these effects influence the intraturbine wake turbulence coupling, Equation (23) ensures that the minimum wake turbulence is equal to the ambient turbulence intensity level. Applying this correction yields the results presented in Figure 9 for the modified DWM model. The main difference occurs in the far-wake region at high turbulence intensities, where the deviations are significantly smaller than in Figure 8 and allows for a more realistic coupling of turbulence intensity to the downstream turbines.

2.2. The effect of the proposed DWM model improvements

The influence of the proposed atmospheric shear contribution and turbulence build-up is examined by simulating flow through a row of eight wind turbines. The wind speed is 8 m s^{-1}, the turbulence intensity is 6% and the mean flow direction is along the row of turbines. We studied two different turbine spacings: 6 D and 10 D.

Figure 10 shows the effect on power output of the individual turbines as the various effects in the DWM model are enabled and disabled. By comparing the power output for the row of turbines when all DWM effects are enabled (black solid lines) to the output if turbulence build-up is not considered (dot-dashed black lines), it is apparent that the effect of turbulence build-up is sensitive to turbine spacing. At 6 D spacing, turbulence build-up has an effect on the wake loss that is twice as large as the effect of wake meandering, but with 10 D spacing, the effect is only about 55% of that caused by wake meandering. The effect on power caused by the atmospheric shear contribution to turbulence is about 5% and 20% of the effect of wake meandering at 6 D and 10 D, respectively. Compared with the total power losses due to wake effects of the unmodified DWM model, the inclusion of wake-added turbulence and turbulence build-up over the row of turbines reduced the predicted wake losses by 9% for the 6 D case and 6% for the 10 D case. The atmospheric shear contribution to turbulence in the DWM model further reduced the power loss by about 0.8% at 6 D spacing and 1.5% for the 10 D case.

These findings show that the proposed DWM model improvements have significant effects on the DWM deficit development. They not only influence the wake turbulence (which is the direct effect) but they also affect the mean wind speed and thereby power predictions. Table I shows the development of turbulence intensity and wind speed along the rows for the two presented cases. The results suggest that an equilibrium wind speed is reached already at the second or third turbine inside the park. The turbulence requires much longer to become fully developed, and an equilibrium value is not reached before the fifth or sixth turbine. This suggests that an approach in which only the nearest upstream wake deficit affects a given turbine might be an acceptable simplification. However, for an accurate turbulence representation, the influence of more upstream wakes should be considered.

2.3. Lillgrund wind farm

The performance of the suggested DWM improvements are tested against field data and OpenFOAM AL results for the offshore Lillgrund wind farm. The power production of the Lillgrund wind farm is estimated by both the unmodified and the modified DWM models and compared with the field data presented by Dahlberg[26] and the OpenFOAM simulations

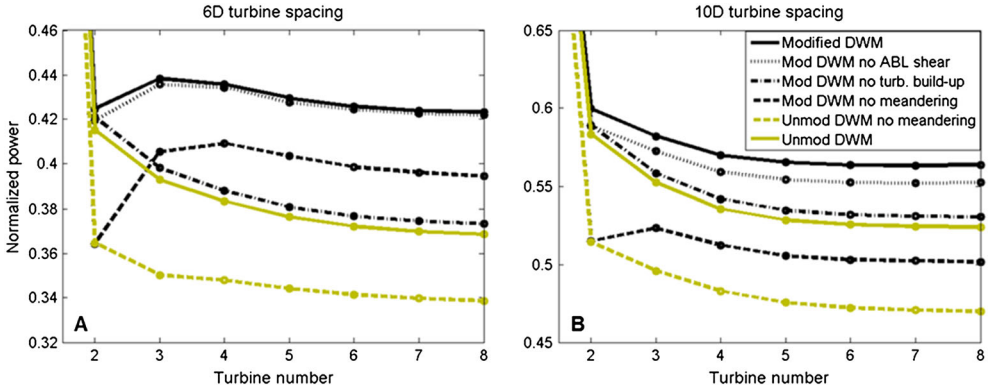

Figure 10. A and B illustrates the individual effect of the DWM model functionalities by showing the predicted power output of eight wind turbines operating in a row aligned with the mean wind direction at 6 D (A) and 10 D (B) spacings with various effects enabled.

Table I. The development of turbulence intensity and wind speed over the row of wind turbines with the proposed atmospheric shear effect and wake turbulence build-up.

Mean wind speed ($m\,s^{-1}$)	WTG 1	WTG 2	WTG 3	WTG 4	WTG 5	WTG 6	WTG 7	WTG 8
6D	8.00	5.90	6.00	6.00	5.97	5.95	5.95	5.95
10D	8.00	6.65	6.62	6.57	6.55	6.54	6.54	6.54
Turbulence intensity (%)	WTG 1	WTG 2	WTG 3	WTG 4	WTG 5	WTG 6	WTG 7	WTG 8
6D	6.0	12.1	13.4	13.9	14.3	14.5	14.6	14.7
10D	6.0	9.7	10.1	10.3	10.4	10.5	10.6	10.6

The ambient conditions for both cases were $8\,m\,s^{-1}$ wind speed and 6% turbulence intensity.

of Churchfield *et al.*[27] The wind speed and turbulence fields of the DWM models were compared with the OpenFOAM data, and the agreement between the two models was evaluated by using Equation (16).

To simulate the Lillgrund wind farm with the DWM model, the rotor induction for the turbines is required. Since this information is not publically available, an approximate rotor description was developed on the basis of the publically available power curve and blade profile family. This rotor description is used in the OpenFOAM AL simulation of the wind farm. The induction vector used in the DWM model for the Lillgrund turbines is based on the time-averaged velocity field at the rotors in the OpenFOAM simulation. First, the velocity field at the rotor is time-averaged and transformed from the Cartesian grid to a vector of axisymmetric values. Then, the azimuthally averaged induction vectors required by the DWM model are found by dividing the axisymmetric velocity vector at the rotor by the oncoming wind speed. For the first rotor, the ambient wind speed is used. For the wake-affected turbines, the oncoming wind speed is found by running a DWM simulation for a single rotor and calculating the mean wind speed at the location of the downstream turbine using Equations (21) and (22).

The layout of the Lillgrund wind farm is shown in Figure 11(a). The analysis presented in this paper is performed for rows B (turbines 15–8) and D (turbines 30–24). Row B contains eight wind turbines that are equidistantly spaced 4.4 D apart. Row D contains seven wind turbines separated by 4.4 D; however, the turbine that would have been the fourth in this row was omitted from the actual wind farm because the water depth is too shallow to allow access by construction boats, so there is an 8.8 D gap between turbines 28 and 27.

The simulations are run in a neutral atmosphere (although there is a stable capping inversion at roughly 800 m above the surface), with a mean wind speed of $9\,m\,s^{-1}$ and a turbulence intensity of 6.2%. The mean flow direction is perpendicular to the rows. The OpenFOAM data is based on a full-scale simulation of the entire wind farm. The duration of the AL simulation is a trade-off between computational cost and uncertainty in the resulting flow field. As a 'standard' AL simulation over the wind farm requires on the order of 500,000 CPU-hours to simulate the flow field for a 10 min period, the simulations times were required to be kept around 10 min to maintain acceptable time consumption with the computational resources available. As shown in Figure 11(b), a consequence of the relatively short simulation time is that the average

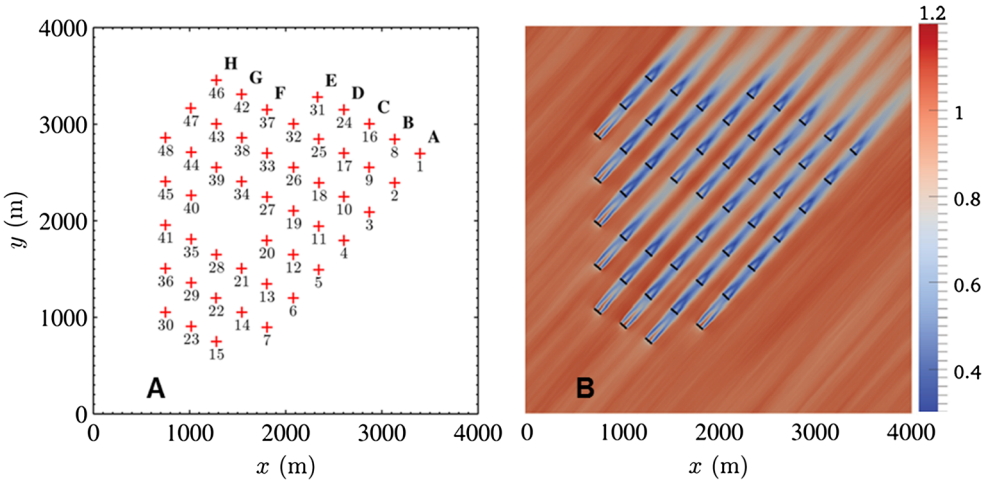

Figure 11. Layout of Lillgrund wind farm (A) and mean wind speed distribution from the OpenFOAM simulation at a hub height of 65 m (B).

DOI: 10.1002/we

wind speed approaching the turbines was not entirely uniform in the whole domain. In the figure, streaks of lower (higher) mean wind speed are seen as lighter (darker) areas. An example of a low-velocity streak that could have some influence on the results is hitting turbine 15 (i.e. the first turbine of row B). This inhomogeneity of the incoming flow field should be seen as a source of uncertainty on the order of $0.165\,\mathrm{m\,s^{-1}}$ in terms of wind speed and 0.53 pp in terms of turbulence intensity. This corresponds to the spatial standard deviation of the average wind speed and turbulence intensity upstream of the wind farm.

A second term of uncertainty due to the short averaging time is the misalignment of the wake deficits, relative to the mean wind direction, because of the stochastic wake meandering (Figure 12). This uncertainty component, $\sigma_{\mathrm{misalignment}}$, is estimated using Equation (31),

$$\sigma_{\mathrm{misalignment}} = \frac{\sigma_{M\frac{d\theta}{dr}}}{\sqrt{n}} \tag{31}$$

where n is the number of independent samples of wake centre position, σ_M is the wake meandering given as the standard deviation of the wake centre position and $\frac{d\theta}{dr}$ is the radial gradient of the studied parameter (for this application axial velocity or turbulence intensity). An estimation of the uncertainty is obtained by assuming the following: (i) 100 independent samples of wake centre position over the 10 min simulations, (ii) a representative standard deviation of the wake centre position equal to 11.2 m (based on simulations by Keck *et al.*[17]), (iii) a wake velocity gradient of $0.06\,\mathrm{m\,s^{-1}\,m^{-1}}$ and turbulence intensity gradient of $0.25\,\mathrm{pp\,m^{-1}}$. Applying these numbers in Equation (31) yields an uncertainty of $0.067\,\mathrm{m\,s^{-1}}$ in terms of wind speed and 0.28 pp in terms of turbulence intensity. However, the average wake deficit and turbulence profiles due to the turbines are still on an order of magnitude larger than the combined uncertainty caused by the low averaging time, which allowed for a high-quality comparative analysis.

The uncertainty in terms of power production is based on the combined root-square sum of the aforementioned sources of uncertainties in wind speed (which is equal to $0.178\,\mathrm{m\,s^{-1}}$). The uncertainty in the power production is estimated as the ratio of power production based on the mean wind plus the combined uncertainty of the wind speed, to power production based on the mean wind speed alone. This yielded an uncertainty in power production of 6%.

By comparing the power production estimates presented in Figure 13, we see that the unmodified DWM model (red lines) predicts lower power production under multiple wake conditions compared with the modified DWM model (black lines). This prediction is expected, as the turbulence build-up in the modified DWM model will lead to a faster wake recovery. Compared with the OpenFOAM AL model (green lines) and the field data (blue lines), the unmodified DWM model under-predicts power production of the row of turbines.

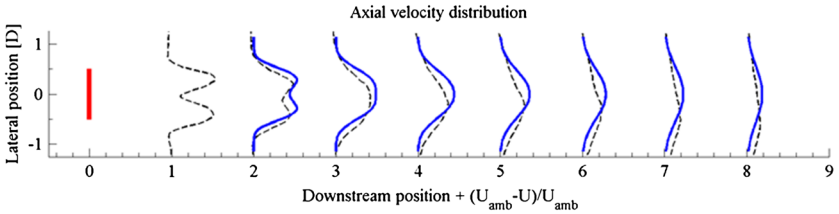

Figure 12. The misalignment of the mean wake deficit of the DWM model (solid lines) and the AL model (dashed lines) behind the first turbine because of relatively short AL simulation times. For the presented case, this misalignment is the main contributor to the resulting STE.

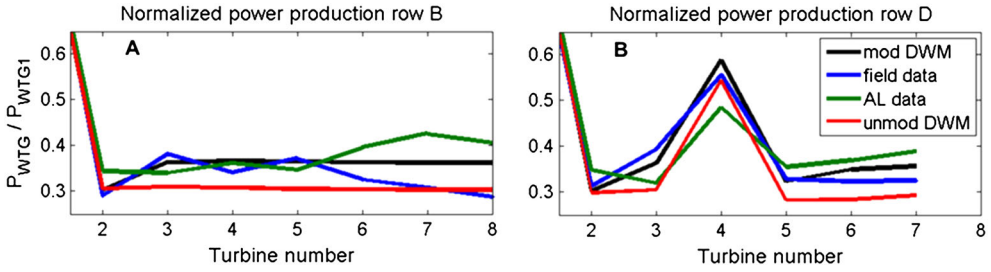

Figure 13. Power production of the wake-affected turbines at row B (A) and D (B) at the Lillgrund wind farm. The green lines are OpenFOAM results, blue lines are field data and black and red lines are the DWM prediction with the modified and unmodified versions, respectively.

In general, the power prediction made by the modified DWM model agrees with the OpenFOAM AL model and the field data. The main deviation seen is the power estimation for the fourth turbine in row D, i.e. the turbine with a larger separation to the upstream turbine, where the DWM model increases slightly more than the OpenFOAM AL model and the field data. We also see that both the modified DWM model and the OpenFOAM AL model overpredict power production for the last three turbines in the rows, compared with the field data. A likely explanation for these deviations is that the field data contain some effect that is not included in the numerical simulations. The DWM model code was run with the same input as the OpenFOAM simulation, which was a neutrally stratified atmosphere with a wind speed of $9.0\,\mathrm{m\,s^{-1}}$ and a turbulence intensity of 6.2%. Although the simulations matched the observed average inflow wind speed and turbulence intensity for this wind direction, the difference in predictions for the rear of the wind farm may be caused by the fact that the field data was collected over many months. Over that period, there was undoubtedly a range of atmospheric stability and wind speed, unlike in the fixed condition simulations. This range may affect the wake propagation and power production. The field data is only binned by wind direction at the first turbine, and wind speeds outside of the turbines' region 2 (in which wake effects are maximum) are not included in the average.

Table II gives a quantitative analysis of the differences in mean wind speed and turbulence intensity distribution over the two rows of turbines. The table shows the STE between the OpenFOAM AL model and the DWM models calculated on the basis of the mean flow field according to Equation (16). The values in the table are based on a single case of ambient conditions: wind speed of $9\,\mathrm{m\,s^{-1}}$ and turbulence intensity of 6.2%. For all turbines, data were collected at the cross sections located 3 and 4 D downstream of the rotor, apart from turbine 3 in row D (i.e. turbine 28 in Figure 11(a)), where data were collected at 3, 4, 5, 6, 7 and 8 D behind the rotor. This is due to the longer undisturbed wake evolution of turbine 28. The data at used in the flow field analysis were collected from along a lateral line at hub height at each cross section. The line was 3.2 D of length, oriented perpendicular to the mean flow direction and centred on the axis of the turbine (thus extending 1.6 D in lateral direction from the mean wake centre).

The two leftmost columns in the tables are the STE between the OpenFOAM AL model and the unmodified DWM model, and the two rightmost columns represent the OpenFOAM AL results compared with the modified DWM model. The table shows that the STE, in terms of mean wind speed, is reduced from 0.73 to $0.51\,\mathrm{m\,s^{-1}}$ for row B (31.1%), and 0.55 to $0.40\,\mathrm{m\,s^{-1}}$ for row D (27.4%). The reduction in STE for turbulence intensity for row B is 3.07 to 1.86 pp (39.4%), and 2.58 to 1.59 pp (38.4%) for row D. Excluding the first turbine, the reduction in STE for waked turbines is found to be 31.8% for wind speed and 43.5% for turbulence intensity, by applying the proposed correction to the DWM model. The STE number should be evaluated with the uncertainty of the AL data in mind. As discussed earlier, the uncertainty of the AL simulations, which is caused by the relatively short simulation times, will increase the STE linearly. The uncertainty, $0.178\,\mathrm{m\,s^{-1}}$ and 0.60 pp for turbulence intensity, could therefore be considered to be the cause of ~39% of the discrepancies in wind speed profiles and ~35% for the turbulence intensity profiles over the rows of turbines.

Note that the STE for the modified DWM model does not increase significantly as a function of turbine position in the row. In fact, the combined STE of the first turbines is actually higher than the mean for the entire row, considering both

Table II. The STE in terms of mean wind speed and turbulence intensity level as a function of turbine position for the modified DWM and unmodified DWM models compared with the OpenFOAM Al model.

	STE WS unmodified	STE TI unmodified	STE WS modified	STE TI modified
	DWM ($\mathrm{m\,s^{-1}}$)	DWM (%)	DWM ($\mathrm{m\,s^{-1}}$)	DWM (%)
WTG 1	0.38	2.11	0.38	2.11
WTG 2	0.51	2.39	0.46	1.81
WTG 3	0.63	2.88	0.40	1.93
WTG 4	0.69	3.48	0.47	2.21
WTG 5	0.80	3.41	0.48	1.78
WTG 6	0.86	2.80	0.55	2.02
WTG 7	0.98	3.21	0.69	1.83
WTG 8	1.02	4.24	0.61	1.18
Mean	0.73	3.07	0.51	1.86
WTG 1	0.60	2.10	0.60	2.15
WTG 2	0.46	1.70	0.43	1.28
WTG 3	0.20	1.54	0.17	1.05
WTG 4	0.55	2.67	0.40	1.50
WTG 5	0.65	3.01	0.43	1.55
WTG 6	0.71	3.62	0.44	1.70
WTG 7	0.68	3.38	0.32	1.88
Mean	0.55	2.58	0.40	1.59

The values are found using Equation (16) and the analysis is carried out for row B (left table) and D (right table).

wind speed and turbulence intensity. The unmodified DWM model has a clear trend of increasing STE numbers with turbine position. Furthermore, by comparing the STE of wind turbine generator (WTG) 3 in row D (i.e. the turbine with the longer undisturbed wake) to the STE of the other turbines, the DWM model agrees better with the AL model at larger downstream distances. The main reason for the increased agreement at downstream is that the gradients of the deficit are smaller, so the comparison is less sensitive to misalignment of the wake centre or difference in the wake width.

The improved agreement between the modified DWM model and the OpenFOAM AL model is also illustrated by showing the turbulence intensity, Figure 14, and mean velocity, Figure 15, at cross sections located 2D, 3D and 4D downstream of turbine 1, 5 and 8 in row B of the Lillgrund wind farm. From the top row of panels (A, B and C), it can be seen that the suggested DWM modifications has little effect on the flow field in a single wake. This is due to the short distances and low turbulence intensity (6.2%), which means that the ABL shear correction has little effect, and since it is the first turbine of the row, the turbulence build-up does not affect the solution.

The middle row of panels (D, E and F) shows that the DWM modification improves the agreement both in terms of wind speed and turbulence intensity when studying the wake after the fifth turbine. In terms of turbulence intensity, Figure 14 shows that the unmodified DWM model (dashed red lines) under-predicts the turbulence in the wake centre and outside of the wake shear layer but overpredicts turbulence intensity of the wake shear layer compared with the AL model. The modified DWM model (solid black lines) overpredicts the turbulence levels in the wake shear layer slightly more than the unmodified model but overall captures the turbulence level outside of the 'peaks' well. The average turbulence intensity level predicted by the modified DWM model is therefore closer than the AL model results. The middle row of Figure 15 shows that the increased turbulence level of the modified DWM model results in a fast recovery, which is closer to that of the AL model. Both DWM implementations overpredict the depth of the deficit in the centre region and under-predict the width of the wake deficit relative to the AL model results.

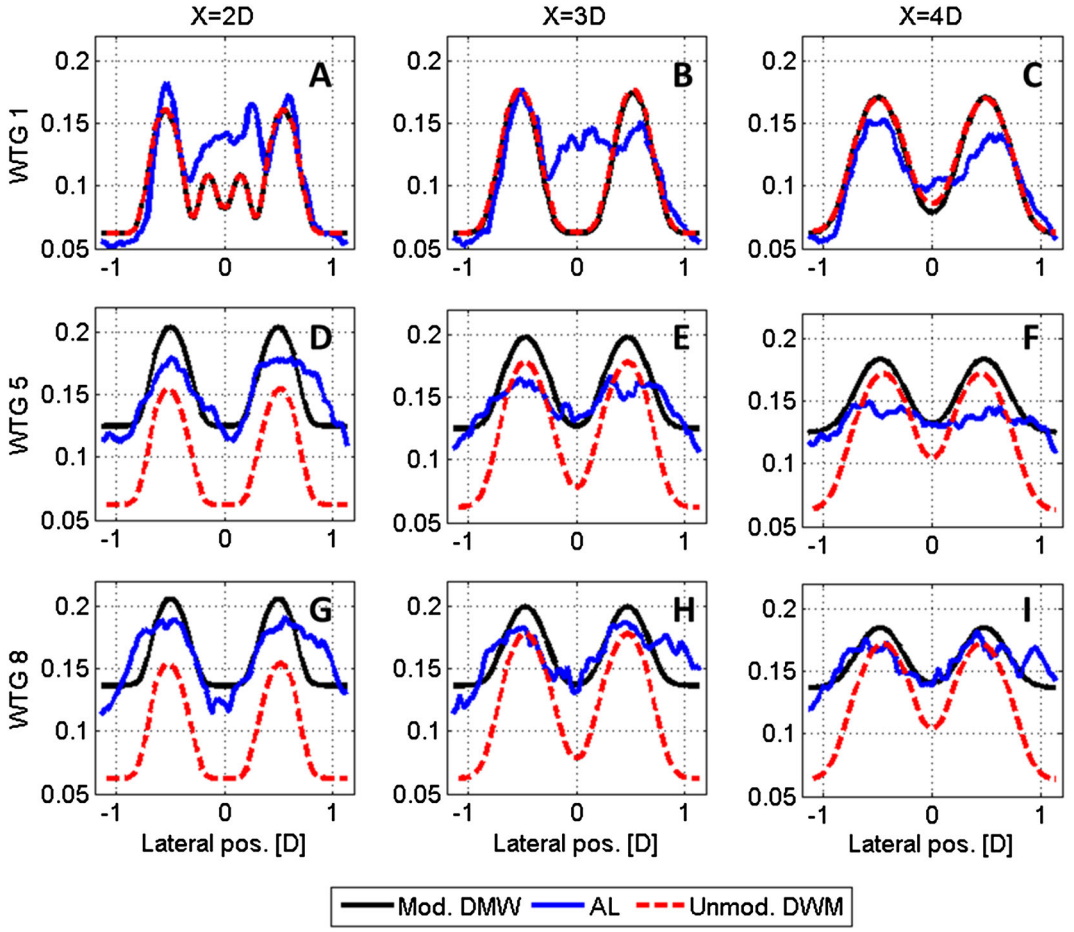

Figure 14. (A–I) The lateral turbulence intensity distribution at hub height of the OpenFOAM model (blue lines), the modified (black lines) and unmodified (dashed red lines) DWM models. The presented data is extracted 2 D (left column), 3 D (middle column) and 4 D (right column) behind the first (top row), fifth (middle row) and eighth (bottom row) over row B of the Lillgrund wind farm.

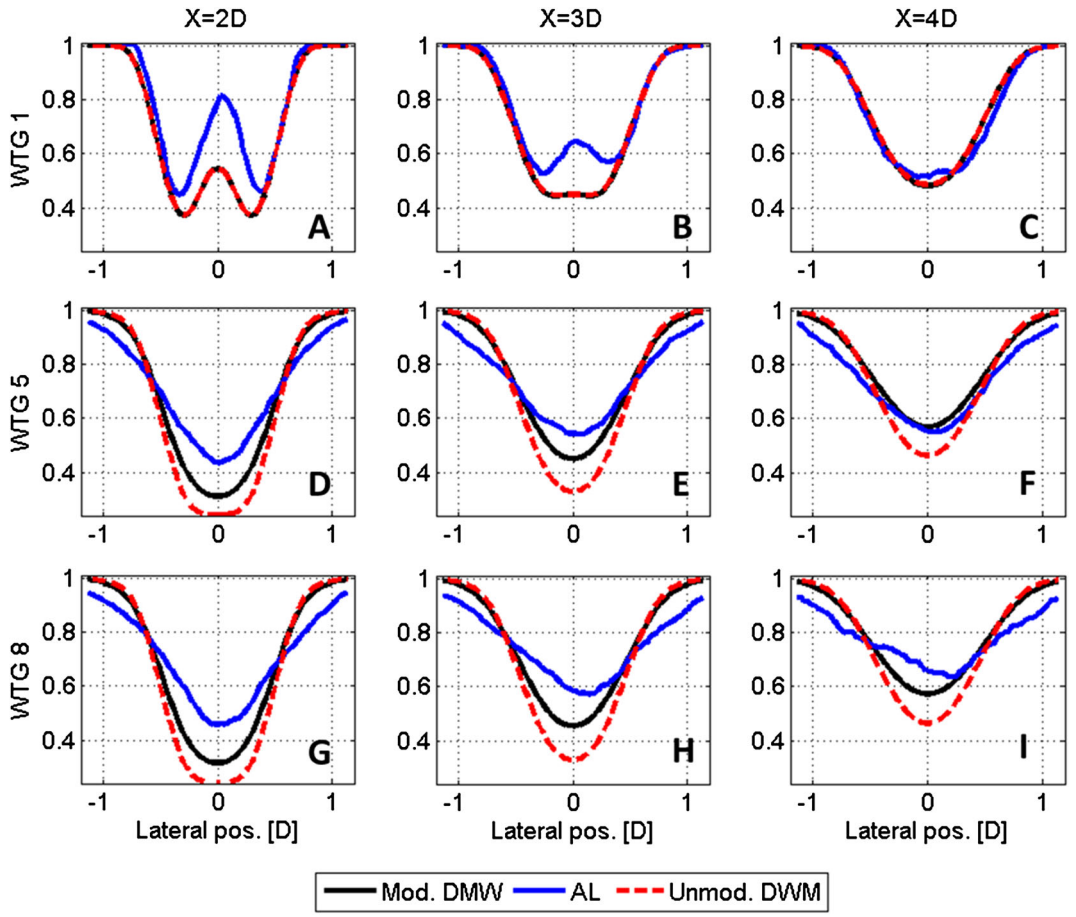

Figure 15. (A–I) The lateral mean velocity distribution at hub height of the OpenFOAM model (blue lines), the modified (black lines) and unmodified (dashed red lines) DWM models. The presented data is extracted 2 D (left column), 3 D (middle column) and 4 D (right column) behind the first (top row), fifth (middle row) and eighth (bottom row) over row B of the Lillgrund wind farm.

The bottom row of panels (G, H and I) shows the same trends as the previously discussed panels (D, E and F). The main differences are that both DWM implementations captures turbulence intensity of the wake shear layer better and that both implementations overpredict the depth of the wake deficit slightly more after the eighth turbine.

It is worth noticing that the wind speed and turbulence fields of the DWM models, compared with the OpenFOAM AL flow fields, also agree fairly well at 2 D (panels A, D and G). This observation suggests that the pressure effects of the upstream rotor are small in that region and that DWM could be valid down to 2 D. The STE at 2 D, however, is roughly four times larger than the STE at 3 D.

3. CONCLUSION

This paper presents a method to include the effect of the vertical atmospheric wind shear in the wake deficit calculation of the DWM model. The main motivation behind the development is that, without the influence of the atmospheric shear, the turbulent stresses used in the DWM model wake deficit diffusion term will be too low in the far-wake region because the wake deficit gradient alone does not yield the representative strain-rate of the local velocity field. As a consequence of the improved far-wake turbulence description, the investigators have also proposed a physically consistent method for modelling the evolution of turbulence over a row of wind turbines.

After investigating the effect on the mean wind field, turbulence distribution and power predictions by the proposed modifications, we conclude that the build-up of wake-added turbulence over the row of turbines and, to a lesser extent, the atmospheric shear contribution to wake turbulence, are significant contributors to the wake recovery process.

The modified DWM model was calibrated on the basis of the results from the Ellipsys3D AL model. The calibration was performed by varying the DWM model coefficients, based on a simplex optimization algorithm, to achieve the best

agreement between the mean velocity field of the DWM model and the Elllipsy3D AL model. The azimuthally averaged velocity field in cross sections located 3 D, 4.5 D, 6 D, 7.5 D and 9 D downstream of the turbine from cases with ambient wind speeds of 6 and 10 m s^{-1}, and turbulence intensities of 6%, 10% and 14%, were used in the calibration. The average normalized deviation between the resulting velocity fields of the two models for all tested cases and cross sections was 0.0162.

The performance of the modified DWM model was evaluated by comparing the results of the DWM models with the results of the OpenFOAM AL model. It was shown that using the modified DWM model resulted in a reduction of the STE between the DWM model and the OpenFOAM AL model. The reduced mean difference in wind speed was on the order of 30%, and the reduced mean difference in turbulence intensity was on the order of 40% for a row of eight turbines. It was also shown that the STE in wind speed and turbulence intensity between the OpenFOAM AL model and the modified DWM model does not increase over a row of turbines compared with the STE seen for a single turbine.

With the proposed model correction, the DWM model now contains a physically consistent method for modelling the development of the wind speed and turbulence field as the wind flows through a row of turbines in a wind farm. As the flow field is physically modelled, the DWM model can be used to extract both loads and power estimations from the same model (this is a capability that other engineering models in the wind industry are lacking). This capability, as well as the fact that the computational speed of the DWM model is maintained at sufficiently low levels to enable design calculations, allows wind farm or wind turbine designers to optimize the performance of both power production and loads simultaneously. Ultimately, this could enable the development of a comprehensive wind farm design philosophy and better wind farm control algorithms.

REFERENCES

1. Madsen HA, Larsen GC, Larsen TJ, Troldborg N, Mikkelsen R. Calibration and validation of the dynamic wake meandering model implemented in the aeroelastic code HAWC2. *Journal of Solar Energy Engineering* 2010; **132**(4): 041014 (14 pages).
2. Ainslie JF. Calculating the flow field in the wake of wind turbines. *Journal of Wind Engineering and Industrial Aerodynamics* 1988; **27**: 213–224.
3. Ainslie JF. Wake modelling and the prediction of turbulence properties. Proceedings of the 8th British Wind energy Association Conference, Cambridge 19–21 March 1986. pp. 115–120, 1986
4. Larsen GC, Madsen HAa, Thomsen K, Larsen TJ. Wake meandering—a pragmatic approach, *Wind Energy* 2008; **11**: 377–395.
5. Madsen HA, Larsen GC, Thomsen K. Wake flow characteristics in low ambient turbulence conditions. In: proceedings of Copenhagen Offshore Wind, 2005.
6. Madsen HA, Larsen GC, Larsen TJ, Mikkelsen R, T roldborg N. Wake deficit-and turbulence simulated with two models compared with inflow measurements on a 2 MW turbine in wake conditions, In: Scientific proceedings. 2008 European Wind Energy Conference and Exhibition, Brussels (BE), 31 Mar–3 Apr 2008. p. 48–53, 2008.
7. Sanderse B. Aerodynamics of wind turbine wakes—literature review. Technical Report ECN-E-09-016, ECN, Netherlands, 2009.
8. Keck RE, Veldkamp D, Madsen HAa, Larsen GC. Implementation of a mixing length turbulence formulation into the dynamic wake meandering model. *Journal of Solar Energy Engineering* 2011; **134**(2): 021012 (13 pages).
9. Sørensen JN, Shen WZ. Numerical modelling of wind turbine wakes. *Journal of fluids Engineering* 2002; **124**(2): 393–399.
10. Sørensen NN. General purpose flow solver applied to flow over hills, Ph.D. thesis, Risø-R-827(EN), 1995.
11. Mikkelsen R. Actuator disc methods applied to wind turbines, MEK-FM-PHD 2003–02. Technical University of Denmark, 2003.
12. Troldborg N. Actuator line modeling of wind turbine wakes, MEK-FM-PHD 2008–06, Technical University of Denmark, 2008.
13. OpenFOAM, Ver. 2.0.x, Silicon Graphics International Corporation (SGI), http://www.openfoam.org/git.php.
14. Churchfield MJ, Lee S, Michalakes J, Moriarty PJ. A numerical study of the effects of atmospheric and wake turbulence on wind turbine dynamics. *Journal of Turbulence* 2012; **13**(14): 1–32.
15. Mikkelsen R, Sørensen JN, Troldborg N. PWSM combined with the actuator line technique. In proceedings of the 2007 EWEC conference, Milan, 2007.
16. Troldborg N, Sørensen JN, Mikkelsen R. Actuator line simulation of wake of wind turbine operating in turbulent inflow. Journal of Physics: Conference Series. The Science of Making Torque from Wind. Technical University of Denmark, Lyngby, 2007.

17. Keck RE, Mikkelsen R, Troldborg N, de Maré M, Hansen KS. Synthetic atmospheric turbulence and wind shear in large eddy simulations of wind turbine wake, accepted for publication April 2013, WE-1631.
18. Mann J. The spatial structure of neutral atmospheric surface-layer turbulence. *Journal of Fluid Mechanics* 1994; **273**: 141–168.
19. Mann J. Wind field simulation. *Probabilistic Engineering Mechanics* 1998; **13**(4): 269–282.
20. Keck RE, de Maré M, Churchfield MJ, Lee S, Larsen GC, Madsen HA. On atmospheric stability in the dynamic wake meandering model, re-submitted after minor revision Journal of wind energy June 2013, WE-13-0020.R1.
21. Ratto CF. Section 1, in Modelling of Atmospheric Flow Fields International Atomic Energy Agency: Vienna, Austria, 1996; 16–18.
22. Gonzalez RC, Woods RE. Digital image processing, Addison-Wesley Reading Mass., 1992
23. Lagarias JC, Reeds JA, Wright MH, Wright PE. Convergence properties of the Nelder–Mead simplex method in low dimensions. *SIAM Journal of Optimization* 1998; **9**(1): 112–147.
24. Matlab User Guide, topic. Optimizing nonlinear functions.
25. Larsen GC, Madsen HA, Larsen TJ, Troldborg N. Wake modeling and simulation. Risø-R-1653(EN). Risø National Laboratory. Technical University of Denmark: Roskilde, Denmark, 2008.
26. Dahlberg J-Å. Assessment of the Lillgrund wind farm: power performance wake effects, [online report] Vattenfall Vindkraft AB, 6_1 LG Pilot Report, Sept. 2009, URL:
27. Churchfield MJ, Lee S, Moriarty PJ, Martinez LA, Leonardi S, Vijayakumar G, Brasseur JG. A large-eddy simulation of wind-plant aerodynamics, AIAA paper 2012–537, 50th AIAA Aerospace Sciences Meeting, Nashville, TN, 2012.